



# Lithological control on the landscape form of the upper Rhône Basin, Central Swiss Alps

Laura Stutenbecker<sup>1</sup>, Anna Costa<sup>2</sup>, and Fritz Schlunegger<sup>1</sup>

<sup>1</sup>Institut für Geologie, Universität Bern, Baltzerstrasse 1+3, 3012 Bern, Switzerland

<sup>2</sup>Institut für Umweltingenieurwissenschaften, ETH Zürich, Stefano-Franscini-Platz 3, 8093 Zurich, Switzerland

*Correspondence to:* Laura Stutenbecker (laura.stutenbecker@geo.unibe.ch)

Received: 21 August 2015 – Published in Earth Surf. Dynam. Discuss.: 2 October 2015

Revised: 12 February 2016 – Accepted: 29 February 2016 – Published: 17 March 2016

**Abstract.** The development of topography depends mainly on the interplay between uplift and erosion. These processes are controlled by various factors including climate, glaciers, lithology, seismic activity and short-term variables, such as anthropogenic impact. Many studies in orogens all over the world have shown how these controlling variables may affect the landscape's topography. In particular, it has been hypothesized that lithology exerts a dominant control on erosion rates and landscape morphology. However, clear demonstrations of this influence are rare and difficult to disentangle from the overprint of other signals such as climate or tectonics.

In this study we focus on the upper Rhône Basin situated in the Central Swiss Alps in order to explore the relation between topography, possible controlling variables and lithology in particular. The Rhône Basin has been affected by spatially variable uplift, high orographically driven rainfalls and multiple glaciations. Furthermore, lithology and erodibility vary substantially within the basin. Thanks to high-resolution geological, climatic and topographic data, the Rhône Basin is a suitable laboratory to explore these complexities.

Elevation, relief, slope and hypsometric data as well as river profile information from digital elevation models are used to characterize the landscape's topography of around 50 tributary basins. Additionally, uplift over different timescales, glacial inheritance, precipitation patterns and erodibility of the underlying bedrock are quantified for each basin.

Results show that the chosen topographic and controlling variables vary remarkably between different tributary basins. We investigate the link between observed topographic differences and the possible controlling variables through statistical analyses. Variations of elevation, slope and relief seem to be linked to differences in long-term uplift rate, whereas elevation distributions (hypsometry) and river profile shapes may be related to glacial imprint. This confirms that the landscape of the Rhône Basin has been highly preconditioned by (past) uplift and glaciation. Linear discriminant analyses (LDAs), however, suggest a stronger link between observed topographic variations and differences in erodibility. We therefore conclude that despite evident glacial and tectonic conditioning, a lithologic control is still preserved and measurable in the landscape of the Rhône tributary basins.

## 1 Introduction

### 1.1 Motivation for this study

The world's topographies have been formed by rock uplift, which is initiated by lithospheric processes such as plate convergence, collision and crustal thickening (England and Molnar, 1990). However, topographic growth on Earth is not indefinite but limited by erosional feedback mechanisms. Once threshold topography has been reached, any further rock uplift (material input) will be balanced by denudation (material output), and this concept is known as topographic steady state (see, e.g., Adams, 1980; Stüwe et al., 1994; Willett and Brandon, 2002). In order to understand this interplay, it is crucial to explore the mechanisms controlling erosion in an area. In this context, several studies have illustrated that denudation and landscape form are highly variable in space and time and that the related topographies depend on a large number of variables, such as climate, glaciation, tectonics and lithology. For example, climate and denudation are coupled in such a way that increased precipitation yields higher river discharges, which in turn tend to enhance rates of fluvial channel incision (see, e.g., Willett, 1999; Willett et al., 2006). Rainfall intensity, paired with the total amount of precipitation, plays an important role in erosional processes by driving hillslope erosion (see, e.g., Wischmeier, 1959) and by contributing to the triggering of mass wasting events that are responsible for mobilizing large amounts of sediment (see, e.g., Bennett et al., 2012). Glacial carving was found to be even more efficient than fluvial erosion, particularly where glaciers have relatively high sliding rates and high basal shear stresses and where subglacial water pressure gradients are large (see, e.g., Hallett et al., 1996; Montgomery, 2002; Norton et al., 2010a, b; Spotila et al., 2004; Shuster et al., 2005; Valla et al., 2011; Jansen et al., 2014; Dürst Stucki et al., 2012). This seems to be especially valid for the Quaternary period, when multiple glacial advances and retreats formed the mountainous landscapes in many orogens (see, e.g., Kelly et al., 2004). On an orogen-wide scale, other authors have reported that the tectonic control on denudation and landscape form has been more pronounced than climate. For example, periods of accelerated uplift in the Alps around 5 million years ago, recorded by apatite fission-track ages (Michalski and Soom, 1990; Vernon et al., 2008; Fox et al., 2015), coincide with a generally higher sediment flux into the foreland basin (Kuhlemann et al., 2002). Besides a possible climatic driver, deep-crustal processes such as unbending and unloading of the subducting slab have been taken into account to explain this large-scale phenomenon (Sue et al., 2007; Baran et al., 2014; Fox et al., 2015). Wittmann et al. (2007) measured Holocene erosion rates in Alpine river sediments, which correlate very well with geodetically based rock uplift rates. These relationships have been used to suggest that vertical movement of rock has mainly been caused by isostatic compensation of removed material (Champagnac

et al., 2009). In thematically related studies, several authors concluded that erosion rates directly correlate with geomorphological variables like slope gradients and local- as well as basin-scale relief that can be extracted from digital elevation models (Granger et al., 1996; Schaller et al., 2001; Montgomery and Brandon, 2002). Finally, lithology and related rock-mass strengths have been considered as additional factors controlling denudation and particularly landscape forms, since soft lithologies like marls are eroded faster than hard lithologies such as granites or gneisses and since mechanically stronger rocks can sustain steeper slopes (see, e.g., Molnar et al., 2007; Korup and Schlunegger, 2009; Korup and Weidinger, 2011; Korup, 2008; Morel et al., 2003; Cruz Nunes et al., 2015; Scharf et al., 2013).

The Central European Alps have been intensively studied regarding how surface and crustal-scale processes have been coupled through time and how effects related to these mechanisms have been modulated by glacial erosion and deposition (see, e.g., Persaud and Pfiffner, 2004; Gudmundsson, 1994; Champagnac et al., 2007; Schlunegger and Hinderer, 2001; Cederbom et al., 2011; Norton et al., 2010b; Schlunegger and Norton, 2013). However, much less attention has been paid to exploring how the tectonic architecture, and the nature of the bedrock lithology in particular, has driven surface erosion and has conditioned the shape of the Alpine landscape (Kühni and Pfiffner, 2001; Norton et al., 2010b), mainly because the spatial and temporal variability of uplift, climate, glacial cover and lithology (Schmid et al., 1996; Kühni and Pfiffner, 2001; Bini et al., 2009) complicates an integrated understanding of the erosional patterns and the resulting landscape form in this orogen. Nevertheless, because of the obvious spatial variation in bedrock lithology, the Alps offer an ideal laboratory to explore whether landscape properties on the basin scale (mean elevation, hypsometry, relief, hillslope gradients and stream profile shapes) are mainly grouped around identical lithologies or around other conditions and driving forces (long- and short-term uplift, climate, etc.). It is the aim of this paper to explore these possibilities.

Here, we focus on the upper Rhône Basin in southwestern Switzerland, which is the largest inner-Alpine drainage system, with a total catchment size of around 5500 km<sup>2</sup>. The Rhône Basin was covered by some of the thickest Alpine glaciers during multiple glaciations throughout the Quaternary (Kelly et al., 2004; Bini et al., 2009) and has recently experienced some of the highest uplift rates in the Alps (Kahle et al., 1997; Schlatter et al., 2005). In particular, we test whether the major spatially variable attributes that have been used to characterize a topography on the basin scale, including mean elevation, relief, slope, hypsometry and longitudinal profiles of streams, bear information that can be related to any of the variables conditioning or controlling erosion, including uplift across timescales, climate, Last Glacial Maximum (LGM) glaciation and lithology. To this extent, we compile topographic data from around 50 tributary basins feeding the Rhône River between its source, the

Rhône glacier, and its terminus, defined here as the delta at Lake Geneva (Fig. 1). We complement our topographic data with published large-scale geological, climatic, glacial (LGM thickness) and exhumation data in order to attain a large-scale understanding of the predominant processes controlling the landscape's form of this basin over multiple scales. We find distinct spatial differences in the landscape's properties, which can be related to the erodibility of the bedrock. This suggests that underlying lithology has exerted a fundamental control on erosion and the resulting landscape form.

## 1.2 Organization of the paper

We base our analyses on previous studies where uplift (long- and short-term), glacial inheritance, precipitation and erosional resistance of the underlying bedrock have been invoked to explain the landscape's characteristics, expressed through variables such as mean elevation, hypsometry, relief, hillslope gradients and longstream profiles (Kühni and Pfiffner, 2001; Wittmann et al., 2007; Norton et al., 2010b; Schlunegger and Norton, 2013; Snyder et al., 2000). We test these relationships through correlation and statistical analyses, and we conclude that variations in erodibility explain most of the morphometric variations that we can observe within the Rhône Basin.

## 2 Geological setting

### 2.1 Geology

The study area covers the entire upper Rhône catchment between the Rhône glacier and Lake Geneva in the Central Swiss Alps (Fig. 1).

The bedrock of the upper Rhône Basin comprises the major tectonic units of the western Alpine orogen (see, e.g., Froitzheim et al., 1996; Schmid et al., 2004). Along its c. 160 km long course from its source next to the Grimselpass at over 2000 m a.s.l. towards the delta on Lake Geneva at c. 370 m a.s.l., c. 50 major tributary streams with sources in either Penninic units, Helvetic nappes or crystalline basement rocks derived from the European continental and oceanic lithosphere (Schmid et al., 2004) discharge their material into the Rhône River. The related lithologies are oceanic metasedimentary and ophiolitic rocks exposed in the Penninic nappes covering 52 % of the total Rhône watershed. These units are mostly drained by tributaries south of the main Rhône valley (Fig. 2a). Variscan crystalline rocks of the European basement (granites, gneisses and schists) of the Aar, Aiguilles Rouges and Mont Blanc external massifs, exposed on both the eastern and western sides of the Rhône valley, contribute to 22 % of the bedrock underlying the Rhône Basin. Calcareous metasedimentary rocks of the European continental margin are exposed in the Helvetic and Ultrahelvetic nappes north of the main Rhône valley and make up c. 16 % of the

total watershed. Finally, minor proportions of the Rhône watershed are made of unconsolidated Quaternary (6 %) and Oligocene molasse (1 %) units as well as the “Sub-Penninic” basement nappes of the Gotthard massif (3 %).

Kühni and Pfiffner (2001) reconstructed a large-scale erodibility map for the Swiss Alps, which is mainly based on the geological and geotechnical map of Switzerland (Niggli and de Quervain, 1936). These authors used detailed field observations, frequency of landslides, as well as structural and topographic parameters from the Rhine Basin (Jäckli, 1957) situated in the eastern Swiss Alps for calibration purposes, based on which erodibility classes were assigned to distinct lithologies (Fig. 2b). Lithologies with a very high erodibility are mainly encountered in molasse and flysch deposits. A medium erodibility has been assigned to Mesozoic carbonates that are exposed in, e.g., the Helvetic nappes and Penninic Klippen belt. Paragneisses are considered to have a low erodibility, while the lowest erodibility has been assigned to orthogneisses, amphibolites and granitoid rocks that are currently exposed, e.g. in the Aar massif.

### 2.2 Tectonics

The tectonic setting of the Rhône Basin is dominated by the Rhône–Simplon fault system, where dextral strike-slip movements since early Miocene times have accommodated most of the orogenic extension (Schlunegger and Willett, 1999; Egli and Mancktelow, 2013). Seward and Mancktelow (1994) suggested that faulting also had a normal slip component, which played an important role in the younger exhumation history of the area. The Rhône–Simplon fault is not only the boundary between two different paleogeographic domains but also separates two terrains with significantly different exhumation histories (Michalski and Soom, 1990; Schlunegger and Willett, 1999; Vernon et al., 2008; and references within, Fig. 3a). In particular, south of this fault in the Penninic domain, apatite fission-track ages range between 8 and 20 million years. In contrast, north of the fault in the Aar massif and the overlying Helvetic nappes, related exhumation ages are considerably younger (1.5–12 million years). The external massifs such as the Aar and the Mont Blanc massif were exhumed in Neogene times at a rate of up to 8 km in  $\leq 15$  My (Pfiffner et al., 1997) and therefore show the youngest exhumation ages of c. 1.5–5 Ma (Michalski and Soom, 1990).

Levelling and geodetic surveys revealed that the Rhône Basin has experienced some of the highest uplift rates throughout the entire Alpine orogen during the past years (Kahle et al., 1997; Schlatter et al., 2005). These high uplift rates were related to a combination of ongoing collisional processes (Persaud and Pfiffner, 2004), erosional (Champagnac et al., 2009) and glacial unloading (Gudmundsson, 1994). Uplift rates are highest in the eastern part of the study area ( $1.5 \text{ mm a}^{-1}$ ) and decrease to  $<0.3 \text{ mm a}^{-1}$  towards Lake Geneva (Fig. 3a).

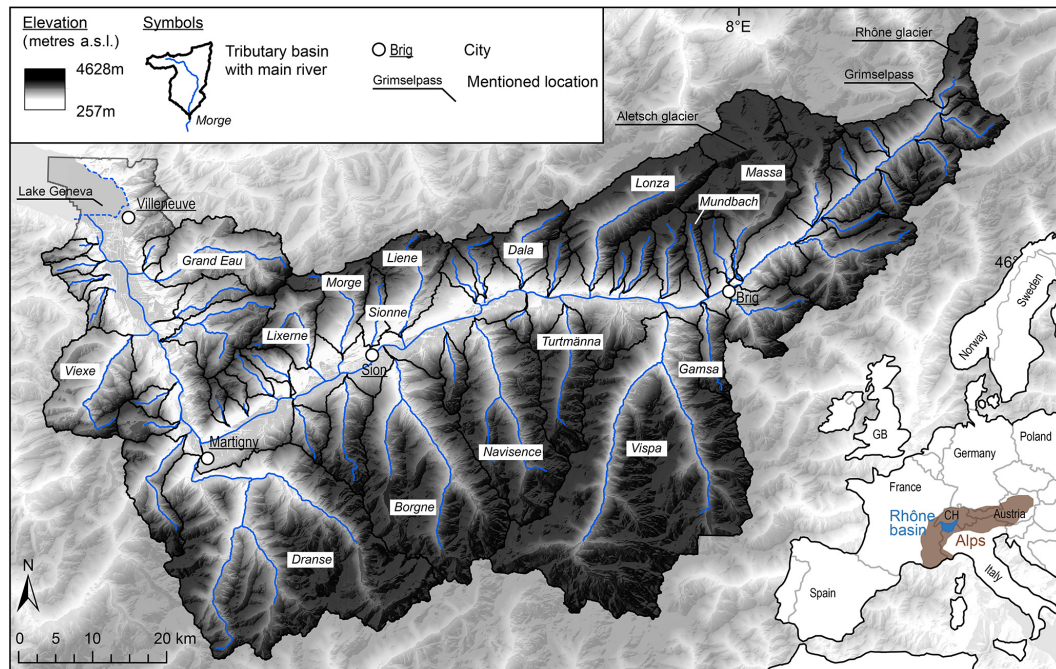


**Figure 1.** Location map of the study area showing the main Rhône River and 55 main tributary streams ( $> 10 \text{ km}^2$ ) that are analysed in this study.

### 2.3 Glaciation

During the Quaternary, the landscape of the Rhône valley was shaped and carved by multiple glaciations (Ivy-Ochs et al., 2008; Valla et al., 2011). In this context, the entire basin was covered by an ice sheet up to 1.5 km thick during the Last Glacial Maximum c. 18–24 ky ago (Kelly et al., 2004; Bini et al., 2009). At the eastern border of the Rhône valley, two separate ice domes formed the ice divide of the Rhône and the Rhine headwaters (Florineth and Schlüchter, 1998). The ice drained into the valleys (including the Rhône valley) down to the foreland in the north, from where the ice thicknesses decreased radially towards the west.

The Rhône valley has hosted some of the thickest Alpine glaciers including the Rhône and the Aletsch glaciers. Today, c. 9 % of the entire upper Rhône watershed is still glaciated, and most of the glaciers are situated in the east and south-east of the basin (Fig. 3b). Their distribution within the three main litho-tectonic units is very distinct, with glacial covers ranging from a maximum of 17.7 % in the Aar massifs to 12.5 % in the Penninic units and only 1.5 % in the Helvetic nappes. Individual tributary basins like the Massa Basin (Fig. 1) are up to 50 % glaciated, whereas others are completely ice-free. Numerous morphological features like oversteepened head scarps, wide, U-shaped, deeply carved trunk valleys and hanging tributary rivers including oversteepened inner gorges reflect the landscape's strong glacial inheritance (Norton et al., 2010a, b; Valla et al., 2011).

### 2.4 Climate

The spatial distribution of precipitation in the current climate is shown in the form of total annual precipitation and high-intensity rainfall represented by annual 90th percentiles of total daily precipitation. Computations are based on the RhiresD product of the Swiss Federal Office of Meteorology and Climatology, MeteoSwiss (Schwarb, 2000). Within the upper Rhône Basin, annual precipitation is characterized by a rather high variability in space, ranging from less than 500 mm per year along the Rhône Valley to more than 2500 mm per year at very high elevations (Fig. 3c). This spatial pattern is mostly driven by orography where inner, low-elevation, sheltered valleys show relatively dry conditions, while the annual amount of precipitation is much larger at higher altitudes (see, e.g., Frei and Schär, 1998).

## 3 Methodology and database

Tectonic, climatic and glacial forcing and their interplay operating on different scales through space and time can be identified by the perturbation they have caused in the landscape. The landscape's response and related morphologic measures can then be suggestive of the extents to which re-equilibrations to those perturbations have proceeded (see, e.g., Robl et al., 2015, for the case of the European Alps). In this context, we extract morphometric data such as elevation, relief, slope, hypsometry and river long profiles from digital elevation model (DEM) distributions to characterize



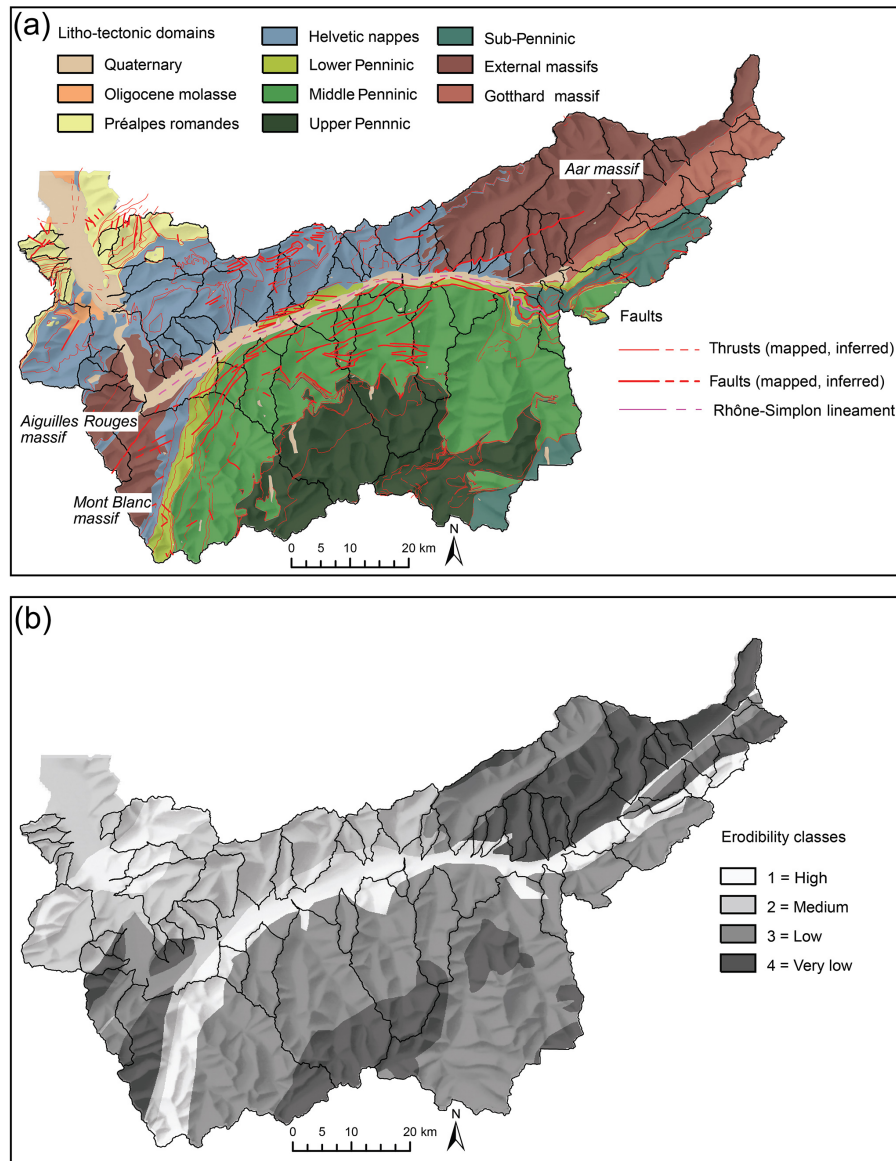


**Figure 2.** Panel (a): simplified litho-tectonic map of the study area showing the major paleogeographic domains, the Helvetic nappes (blue), the Penninic nappes (green) and the external massifs (red) and the major structural features (data compilation from swisstopo<sup>®</sup> geological map 1 : 50 000). Panel (b): erodibility map after Kühni and Pfiffner (2001), based on Niggli and de Quervain (1936) and Jäckli (1957) showing the general erodibility of bedrock.

the landscape on the basin scale (see, e.g., Wobus et al., 2006; Brocklehurst and Whipple, 2004; Champagnac et al., 2012; Robl et al., 2015). We then test the possible relation of these topographic variables to external forcing mechanisms such as uplift, precipitation, glacial inheritance and erodibility through distribution and linear discriminant analyses.

### 3.1 Topographic variables

All topographic variables including measures of elevation, slope gradients and river profile shapes (on the tributary basin scale) were extracted with standard geomorphological and

hydrological tools in ArcGIS<sup>®</sup> version 10.1. The base data set for all analyses was the 2 m resolution DEM swissALTI<sup>3D</sup> generated by the Swiss Federal Office of Topography (swisstopo) in 2014.

#### 3.1.1 Mean elevation, relief and slopes

We calculated mean elevation within each basin from the 2 m resolution DEM.

The local relief corresponds to the difference between the highest and the lowest point of elevation in a defined area (Ahnert, 1984). Because the studied tributary basins have

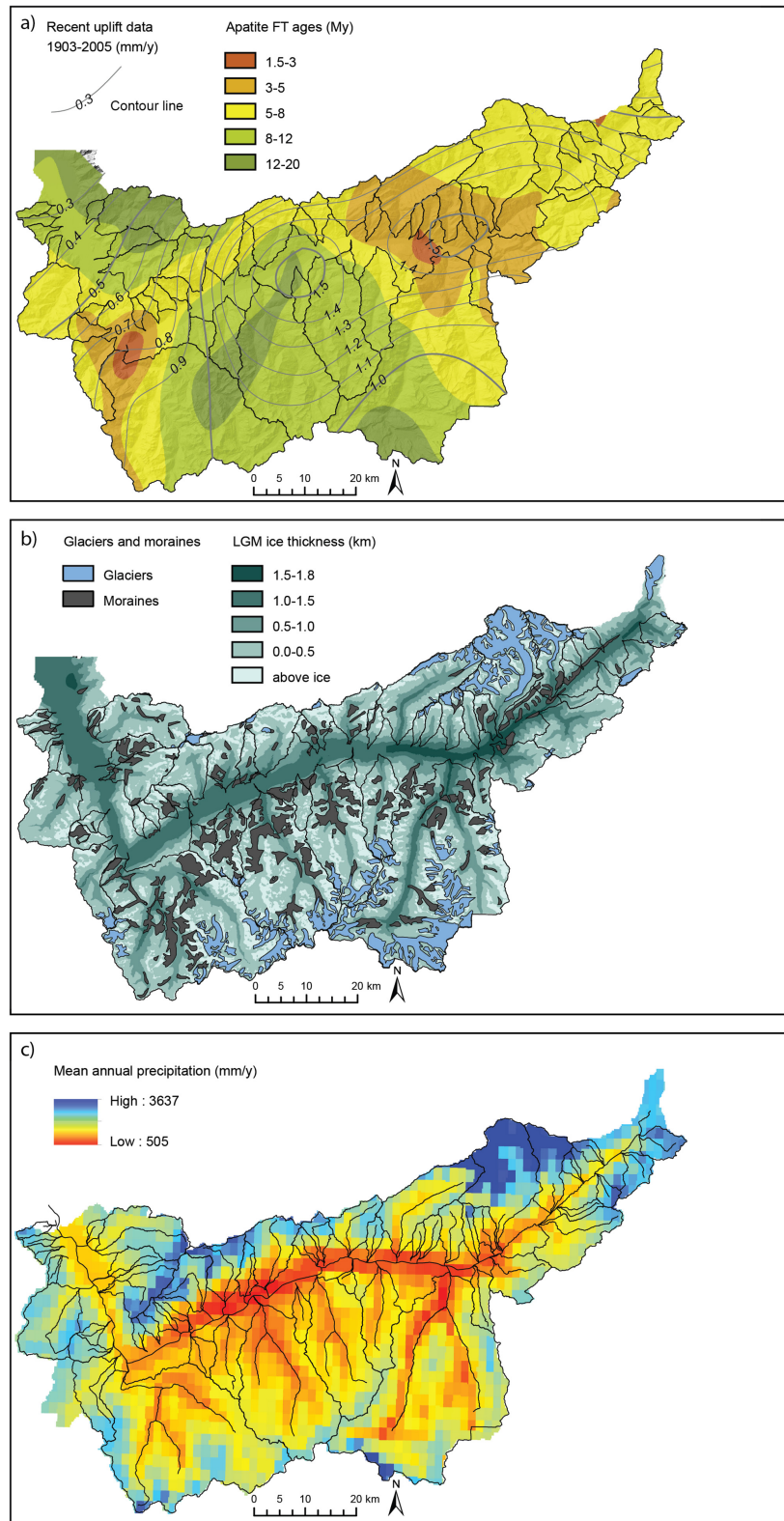


**Figure 3.** Panel (a): interpolated exhumation ages based on apatite fission-track dating (Vernon et al., 2008) show youngest ages both in the east and the west and a decrease towards the basin outlet at Lake Geneva. Contour lines indicating recent uplift (for the time span 1903–2003) are interpolated from Schlatter et al. (2005) and Kahle et al. (1997). Panel (b): map showing the ice thickness during the Last Glacial Maximum (from Bini et al., 2009) and the recent distribution of moraine deposits (glacial till) and glaciers. Panel (c): spatial distribution of total annual precipitation averaged over the period 1961–2012 based on Schwarb (2000).

significantly different catchment sizes (c. 10–700 km<sup>2</sup>), it is not meaningful to calculate the local relief over the entire catchment. For better comparability, we instead chose a 1 km diameter circular sampling window, in which the mean elevation difference is calculated using focal statistics (Montgomery and Brandon, 2002; Korup et al., 2005). Finally, slope values were calculated in ArcGIS® with the imbedded slope algorithm from the 2 m DEM. We excluded currently glaciated areas from the calculation because they would bias the results towards higher frequencies of lower slopes. Mean slope values were then calculated from this database for each tributary basin.

### 3.1.2 Hypsometry

We used the hypsometric integral (Strahler, 1952) as a measure of the distribution of elevations within the catchments. In particular, the hypsometry of a basin can be used to infer the stage to which the landscape has evolved, where progressive erosion will continuously lower the overall topography and elevations will be skewed towards lower values (Strahler, 1952; Brozović et al., 1997). The hypsometric integral (HI) can be expressed as the integral below the hypsometric curve, which in turn represents the proportion of a basin that lies below a given elevation (Hurtrez et al., 1999). The hypsometric curve displays normalized elevations on the ordinate and normalized cumulative area above the corresponding elevation on the abscissa. The convexity of the shape of this curve increases (and corresponding HI values are accordingly higher) as the distribution of elevations are skewed towards higher values. In contrast, s-shaped or concave hypsometric curves and lower HI values occur in more evolved landscapes, where erosional processes have preferentially removed areas of high elevation (Brozović et al., 1997; Brocklehurst and Whipple, 2002, 2004; Montgomery et al., 2001). Accordingly, we calculated the HI for each watershed > 10 km<sup>2</sup> using a bin size of 100 m suitable for hypsometric analyses through Eq. (1):

$$HI = \frac{H_{\text{mean}} - H_{\text{min}}}{H_{\text{max}} - H_{\text{min}}}, \quad (1)$$

where  $H_{\text{mean}}$ ,  $H_{\text{min}}$  and  $H_{\text{max}}$  refer to the mean, minimum and maximum elevation of the basin.

### 3.1.3 River profiles

Several authors have quantified the concavity of longitudinal river profiles (e.g. Whipple and Tucker, 1999; Whipple, 2004; Wobus et al., 2006) through the application of Flint's law (Flint, 1974), where the local channel gradient  $S$  is related to the upstream drainage area  $A$  through Eq. (2):

$$S = k_s \cdot A^{-\theta}. \quad (2)$$

Here, the coefficient  $k_s$  corresponds to the steepness index, while the exponent  $\theta$  is referred to as the concavity index. In

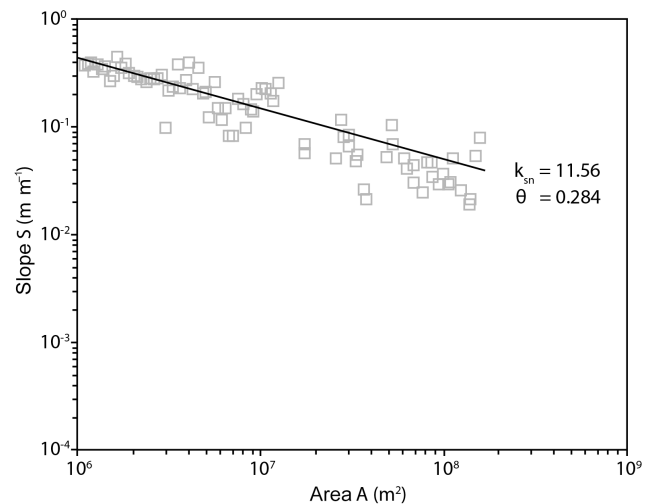


**Figure 4.** Exemplary plot showing the linear regression of the logarithmic slope–area plot, from which the two variables  $\theta$  and  $k_s$  can be derived.

the case of normally graded stream profiles,  $S$  and  $A$  show a linear relationship in log–log plots (Fig. 4). The slope of this linear regression line corresponds to the concavity index  $\theta$ , while the intercept with the y axis is the value of the steepness index  $k_s$ .

Longitudinal river profiles were extracted from the hydrologically filled 2 m DEM provided by Swisstopo using ArcGIS® 10.1 and the Matlab® based TopoToolbox by Schwanghart and Kuhn (2010). The code calculates the hydrologic flow into each pixel and based on this extracts the main channel of the river (i.e. the pixels in which the hydrologic flow is largest). Along the main channel, elevation and distance, as well as slope and upstream area are extracted in order to plot the river profile and the slope–area relation, respectively.  $\Theta$  and  $k_s$  are then calculated through linear regressions of the slope–area plot. We performed this regression over the entire stream length to allow better comparison between the different streams (see, e.g., Korup, 2008).

### 3.2 Possible controlling and conditioning variables

Parameters are referred to as controlling or conditioning variables if they have been used to explain the topographic development of the Rhône drainage basin across scales including uplift (Wittmann et al., 2007), precipitation and/or glacial inheritance (Schlunegger and Norton, 2013) and erodibility (Kühni and Pfiffner, 2001). These variables potentially explain the patterns of first-order morphometric variables outlined above. We assign quantitative values for the four variables to each tributary basin, using published maps as a basis (see Sect. 2).

### 3.2.1 Uplift

We consider two different timescales by exploring the controls of rock uplift on the landscape of the Rhône. First, patterns of long-term exhumation and related rock uplift can be extracted from apatite fission-track cooling ages (Sect. 1.2). Accordingly, for each tributary basin, we calculate mean cooling ages based on the map by Vernon et al. (2008). The tributary basins are then categorized using a ternary division into relatively recent (1.5–5 My ago), intermediate (5–8 My ago) and old (>8 My ago) cooling ages. This division approximately follows the assignment to classes by Vernon et al. (2008).

To account for recent surface uplift rates, we use the data provided by Schlatter et al. (2005), which we interpolated along the study area. This data set is based on geodetic levelling surveys conducted for around 10 000 control points over Switzerland by the Swiss Federal Office of Topography between ~1903 and 2003. We divide recent surface uplift into three intervals including low (0.5–0.9 mm a<sup>-1</sup>), intermediate (0.9–1.4 mm a<sup>-1</sup>) and high (1.4–1.6 mm a<sup>-1</sup>) rates and assign related classes to each tributary basin.

### 3.2.2 Precipitation

The distribution of total annual precipitation (amount) and annual 90th percentiles (intensity) of total daily precipitation are used to characterize modern precipitation rates and patterns, respectively. Computations are based on the RhiresD product of the Swiss Federal Office of Meteorology and Climatology MeteoSwiss (Schwarb, 2000). RhiresD is a gridded daily precipitation data set covering the Swiss territory with a spatial resolution of ~2 × 2 km from 1961 to present. Computations are conducted directly on the native grid and are consecutively distributed over a 250 × 250 m grid by proximal interpolation. The precipitation amount and 90th percentile of total daily precipitation were calculated on an annual basis and averaged over the 52-year period 1961–2012 for each catchment. Quantiles are computed only for wet days, assuming a threshold of 1 mm day<sup>-1</sup> for distinguishing wet and dry days.

For the precipitation amount, we divide the basins into three evenly spaced classes: 975–1340, 1340–1840 and 1840–2278 mm year<sup>-1</sup>. For the precipitation intensity indicated by the 90th percentile, we also divide the basins into three evenly spaced classes: 19–25, 25–31 and 31–37 mm day<sup>-1</sup>.

### 3.2.3 Glacial inheritance

The glacial extent during the LGM and related patterns of ice thickness (Florineth and Schlüchter, 1998; Kelly et al., 2004; Bini et al., 2009) are used, mainly because this variable has been used to explain some of the landscape forms in the Central European Alps (Schlunegger and Norton, 2013). We calculate LGM-related ice volumes within each tributary basin

by subtracting today's landscape elevation (derived from the DEM) from the LGM surface map by Bini et al. (2009). Areas that were above the ice during the LGM are excluded from the resulting map. We calculate mean values of the resulting ice thickness for each tributary basin and classify them into three evenly spaced intervals: 167–292, 292–471 and 471–651 m.

### 3.2.4 Erodibility

We use the erodibility classes defined by Kühni and Pfiffner (2001) (see Sect. 2.1) as a measure of the erosional resistance of the underlying bedrock. Flysch and molasse deposits are assigned a high erodibility (1). Mesozoic carbonates as they occur in the Helvetic nappes have a medium erodibility (2). Paragneisses and other poly-metamorphic rocks that are exposed mainly in the Penninic nappes and subordinately in the external massifs have a low erodibility (3). Very low erodibility values (4) have been assigned to granitoid rocks and orthogneisses. These rock types are common in the external massifs and subordinate in the Penninic nappes. Since most of the basins comprise rocks of different erodibilities (Fig. 2b), we calculate mean values for each basin, thus considering the relative proportion of erodibility classes per basin, and group them into high (1–2), low (2–3) and very low (3–4).

This division would need to be more precise on a smaller scale to allow the consideration of small-scale lithological variation. However, for our basin-wide approach, we found this division sufficiently precise.

## 3.3 Correlation, distribution and statistical analysis

Possible relationships between the topographic and the controlling variables are explored through regression analyses, where correlation strengths for each pair of variables are expressed by the square of the correlation coefficient,  $r^2$ .  $r^2$  values >0.5 are considered to indicate a strong correlation, while values between 0.3 and 0.5 indicate weak correlation. No causal relationships are assigned for pairs with correlation <0.3. Several authors found that some of the topographic measures analysed here may depend on basin size rather than on external forcing mechanisms (e.g. Willgoose and Hancock, 1998; Korup et al., 2005; Cheng et al., 2012). Since the tributary basins in the study area show quite a large range between c. 10 and >700 km<sup>2</sup>, we also test possible dependencies of all topographic variables on basin size.

We then analyse the relation between the topographic and the controlling variables. To achieve this, all topographic variables are plotted in sets of boxplots for each controlling variable. The boxplots display the general range of the data, including the maximum and minimum values, the median, the upper and lower quartile, and outliers. These statistical measures help to describe the general data distribution and their scatter. Furthermore, they allow for the comparison of



the distribution of data between defined classes and help to identify whether there are significant differences.

We finally test whether the topographic variables of the studied basins are sufficient to predict the affiliations of the basins through linear discriminant analyses (LDAs). In contrast to principal component analysis, LDA takes into account the affiliation of a sample to a certain group (McLachlan, 2004), in our case for example basins with similar uplift rates or low erodibility. Therefore, LDA allows us to test whether a basin has been assigned correctly to a group (e.g. high uplift rate) based on its topographic characteristics. In addition, because the LDA reduces the dimensions of the data to a linear space, related results can be displayed in a two-dimensional scatter plot, where each sample is defined by two eigenvectors (McLachlan, 2004). The distinct groups should then be visible as clusters in this plot if the topographic variables are significantly different between the groups of the chosen category. Furthermore, the LDA approach results in the prediction of the affiliation of a sample to a group based on the eigenvalues inferred from the variables, and it allows the comparison of these results with the actual group affiliation.

## 4 Results

### 4.1 Values and correlations

Most topographic variables show a relatively large scatter between the analysed catchments (see Table 1). Mean elevations range between c. 1420 and 2890 m a.s.l.. The mean values of relief calculated for 1 km radii range between 470 and 990 m, while slopes are between 19.5 and 40.7° steep on average. The hypsometric integral has a mean value of 0.45 but scatters widely between 0.28 and 0.70 for the individual tributary basins. The river long profiles also show a wide variety in shape (Fig. 5). They display almost undisturbed concave to s-shaped (concave–convex) with knick-points to almost completely convex profiles. Accordingly, the  $\theta$  and  $k_s$  values yield large scatters. Most important, nearly all river profiles have features indicative of topographic transient states such as multiple knickzones and convexities (Fig. 5).

Most topographic variables show no or only weak correlation ( $r^2 < 0.3$ , see Fig. 6) with one another. Only the pairs of slope–relief and HI– $\theta$  are characterized by a strong positive correlation with values of  $r^2 > 0.5$ . No statistically significant correlations between any of the topographic variables and basin size were observed (all  $r^2 < 0.3$ ).

For the controlling variables, Table 2 shows the extracted values for each basin based on the categorization described in Sect. 3.2. There exists a strong correlation between the two measures of precipitation ( $r^2 = 0.710$ , Fig. 7). Since all other variable pairs have  $r^2$  values below 0.3, they can be considered as not strongly correlated. Note that also for basin size there is no statistically significant correlation between any of the analysed variables (Fig. 7).

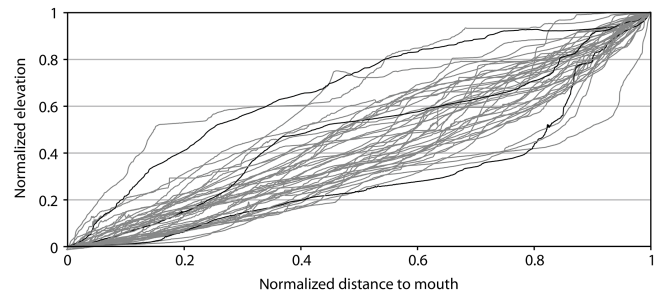


**Figure 5.** Longitudinal river profiles with normalized distance and elevation.

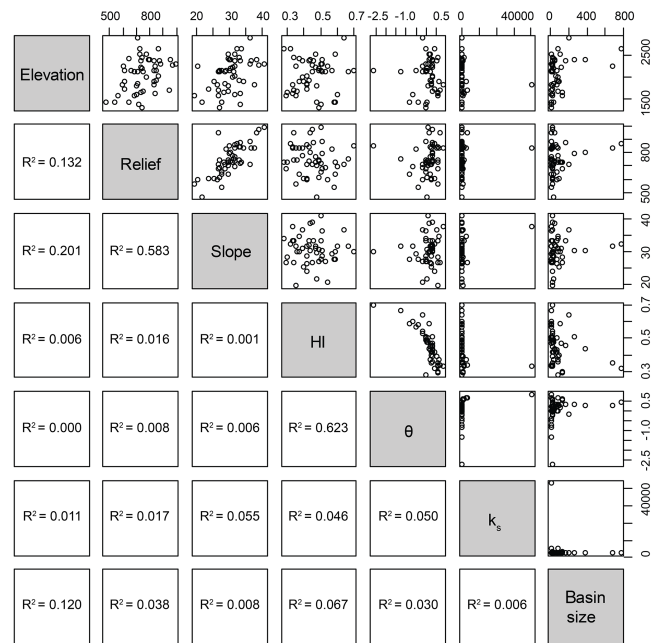


**Figure 6.** Correlation matrix of the topographic variables extracted from the DEM (mean elevation, relief, slope, HI, concavity,  $k_s$ ) and basin size. The strength of correlation for each pair is given by the coefficient of determination,  $r^2$ .

### 4.2 Distribution analysis in boxplots

Each set of boxplots (Figs. 8–13) displays the topographic variables grouped into the three subclasses defined for each of the controlling variables.

The mean apatite fission-track ages for each catchment can be used as a proxy for the long-term uplift history (Vernon et al., 2008). Figure 8 shows that the topographic variables generally fall into these three classes (< 5 My ago, 5–8 My ago and > 8 My ago; see above and Vernon et al., 2008), albeit with a large scatter. Catchments characterized by relatively old apatite ages show generally lower elevation, relief and slope values. Conversely, catchments yielding young apatite ages show the highest values of elevations, relief and slopes. In contrast, hypsometric integrals and river profile shapes do

**Table 1.** Topographic variables (Sect. 2.1) extracted for the studied catchments.

Catchment	Catchment size (km <sup>2</sup> )	Mean elevation (m)	Local relief (m)	Slope (°)	HI	$k_s$	$\theta$
Aegene	36.0	2420.2	641.2	29.8	0.37	0.57	0.18
Avancon	82.6	1676.6	747.7	29.8	0.36	4.05	0.32
Baltschiederbach	42.6	2395.3	949.9	38.4	0.44	0.58	0.11
Bietschbach	21.9	2273.1	973.5	39.0	0.45	3.21	0.29
Binna	116.1	2215.9	729.8	31.0	0.47	16.72	0.31
Blinne	18.3	2371.5	831.5	36.6	0.39	7.85	0.54
Borgne	385.1	2399.1	798.0	30.3	0.44	3.24	0.27
Boverèche	18.6	1732.1	609.5	23.9	0.42	8.56	0.40
Chelchbach	27.1	2112.1	711.5	26.6	0.45	1.24	0.19
Dala	58.5	2036.4	860.5	31.7	0.42	4.48	0.29
Dranse	674.8	2243.7	836.8	31.6	0.35	1.97	0.26
Farne	29.0	1846.8	712.5	28.7	0.42	1.81	0.24
Feschilju	18.1	2133.0	683.5	28.6	0.51	0.13	−0.05
Fossau	11.7	1373.0	717.8	33.3	0.50	0.10	−0.04
Fully	10.4	2149.9	828.6	29.2	0.57	0.00	−0.53
Gamsa	38.5	2199.7	739.8	30.5	0.49	0.25	0.04
Goneri	40.0	2371.9	732.9	31.8	0.43	2.05	0.30
Grand Eau	130.0	1570.4	682.9	26.6	0.29	57.95	0.55
Greffe	10.5	1429.3	641.6	27.7	0.59	0.00	−0.83
Gryonne	34.8	1423.4	471.1	21.7	0.48	0.08	0.01
Illbach	11.0	1816.8	833.0	37.6	0.33	15.06	0.82
Jolibach	11.5	2288.8	882.5	36.2	0.51	0.25	−0.02
Liene	92.3	1910.0	608.2	25.4	0.40	1.43	0.24
Lixerne	64.8	1920.2	843.7	33.1	0.43	1.24	0.21
Lonza	161.5	2361.2	871.5	33.3	0.46	6.09	0.28
Losentse	22.1	1618.0	838.7	33.3	0.33	13.94	0.58
Massa	202.9	2891.1	712.6	36.4	0.64	0.00	−0.18
Milibach2	15.9	2236.5	600.7	20.6	0.54	0.01	−0.22
Morge	72.1	1823.5	598.5	26.4	0.42	1.45	0.21
Mundbach	23.8	2305.8	991.0	40.7	0.50	0.56	0.06
Münstigerbach	15.7	2455.7	743.3	33.1	0.34	143.34	0.59
Navisence	255.8	2389.8	790.9	30.2	0.51	4.42	0.31
Printse	72.1	2137.8	659.2	27.6	0.50	0.09	−0.02
Randonne	11.9	2124.1	749.3	31.5	0.67	0.00	−1.32
Raspille	27.6	2158.4	614.9	27.1	0.49	0.17	0.00
Reche	26.9	2124.9	687.6	27.1	0.53	0.01	−0.21
Salanfe	25.9	2139.4	849.6	30.0	0.70	0.00	−2.69
Salantse	19.9	1804.1	704.9	29.7	0.48	0.53	0.10
Saltina	76.8	2008.3	776.8	30.9	0.39	3.65	0.31
Sionne	26.7	1578.9	561.7	19.6	0.35	8.57	0.54
Torgon	11.2	1441.8	539.2	27.7	0.58	0.00	−0.40
Torrent de Saint-Barthélemy	12.4	1705.5	948.9	26.6	0.34	57.75	0.66
Tove	12.3	1604.9	697.9	31.6	0.60	0.00	−0.71
Trient	83.2	1898.5	832.6	34.4	0.37	57.93	0.63
Turtmäna	108.0	2512.7	725.0	29.8	0.59	1.17	0.15
Viexe	134.8	1651.2	731.2	28.3	0.30	385.20	0.56
Vispa	773.9	2640.8	867.3	32.4	0.32	42.41	0.41
Walibach	12.1	2524.1	773.2	31.6	0.47	1.44	0.19
Wysswasser	84.6	2636.1	727.3	33.8	0.28	0.08	−0.02
Yvorne	10.2	1307.3	744.7	27.1	0.49	0.13	−0.01

**Table 2.** Possibly controlling variables (2.2) extracted for the studied catchments.

Catchment	Apatite FT ages (My ago)	Recent uplift rate (mm year <sup>-1</sup> )	LGM ice thickness (m)	Mean annual precipitation (mm year <sup>-1</sup> )	Annual 90th percentile (mm day <sup>-1</sup> )	Erodibility
Aegene	5.0	1.23	482	2018.0	29.77	2.34
Avancon	8.1	0.67	339	1839.8	28.73	1.78
Baltschiederbach	3.1	1.54	421	1325.4	27.80	3.92
Bietschbach	2.9	1.50	445	1301.7	25.91	3.28
Binna	4.8	1.48	475	1446.7	27.00	2.56
Blinne	5.0	1.37	415	2010.4	32.52	2.14
Borgne	8.9	1.26	281	1097.5	19.95	3.31
Bovereche	5.9	1.39	567	1269.4	25.55	1.82
Chelchbach	3.3	1.51	611	1198.7	30.01	3.99
Dala	3.8	1.28	438	1581.4	28.22	2.00
Dranse	7.1	1.01	364	1332.8	22.42	2.73
Farne	8.0	1.03	275	976.2	19.09	2.09
Feschilju	3.0	1.36	309	1542.7	28.46	2.47
Fossau	8	0.38	348	1794.5	28.46	2.00
Fully	3.8	0.72	164	1663.2	28.49	2.77
Gamsa	3.7	1.36	433	1318.4	25.49	2.89
Goneri	5.0	1.08	591	2104.6	28.47	3.74
Grand Eau	11.5	0.58	292	1675.1	25.26	1.36
Grefe	6.8	0.46	247	1761.4	27.47	1.98
Gryonne	10.8	0.59	344	1521.2	23.61	1.17
Illbach	6.7	1.41	467	1114.2	21.00	1.91
Jolibach	3.0	1.49	367	1258.8	24.92	2.99
Liene	6.2	1.32	396	1433.5	26.60	1.83
Lixerne	6.0	0.93	321	1802.7	30.90	2.00
Lonza	3.8	1.34	424	1507.1	25.31	3.13
Losentse	5.1	0.85	517	1292.5	22.86	2.00
Massa	4.9	1.37	258	2266.7	37.68	3.65
Milibach2	5.0	1.47	423	1557.3	28.20	1.86
Morge	5.9	1.15	417	1734.3	30.75	1.98
Mundbach	3.2	1.54	476	1387.1	31.64	3.99
Münstigerbach	5.0	1.21	413	1940.9	29.93	3.99
Navisence	8.0	1.34	306	1118.6	21.47	3.02
Printse	9.7	1.20	235	1028.6	19.73	2.86
Randonne	5.0	0.74	113	1797.6	30.05	2.47
Raspille	5.0	1.31	389	1667.2	29.83	1.91
Reche	8.9	1.55	194	1011.9	19.75	2.96
Salanfe	3.6	0.65	142	1823.6	30.33	2.83
Salantse	5.0	0.77	273	1610.8	26.90	2.02
Saltina	3.0	1.45	651	1325.7	24.94	2.65
Sionne	6.1	1.34	581	1278.5	25.21	1.73
Torgon	8	0.4	209	1752.8	27.64	2.00
Torrent de Saint-Barthélemy	4.1	0.62	284	1665.1	27.75	2.49
Tove	8	0.3	217	2009.8	31.83	2.00
Trient	4.1	0.81	396	1559.3	27.32	3.34
Turtmäna	6.9	1.34	243	1102.6	21.76	3.14
Viexe	5.0	0.50	307	1709.2	26.86	1.64
Vispa	6.8	1.10	411	1242.4	25.44	3.20
Walibach	5.0	1.33	314	1983.7	34.97	3.98
Wysswasser	5.0	1.34	403	2136.3	37.95	3.92
Yvorne	11.8	0.4	389	1388.8	22.17	2.00

not show any variation between the three sets of fission-track ages.

Short-term uplift rates, which have been quantified using geodetic data collected over the past century (Schlatter et al., 2005), yield a similar pattern regarding relationships with topographic metrics. Elevation, relief and slope values tend to increase with increasing surface uplift rate (Fig. 9a, b, c), although the trend is less clear than in the case of the long-term uplift variable. Hypsometric integrals and the river profile shapes show no clear trend with geodetic uplift rates (Fig. 9 d, e).

Mean ice thickness in each catchment during the LGM can be considered as a measure of glacial imprint onto the landscape (Schlunegger and Norton, 2013). However, no clear variations can be observed between the three defined LGM thickness classes and elevation, relief and slope (Fig. 10a, b, c). In basins with thicker ice, the HI is clearly lower and the river profile concavity higher than in basins with thinner ice (Fig. 10d, e).

Precipitation is quantified by the amount and the intensity of precipitation averaged over the time span from 1961 to 2012, for which a data record is available. Regarding the

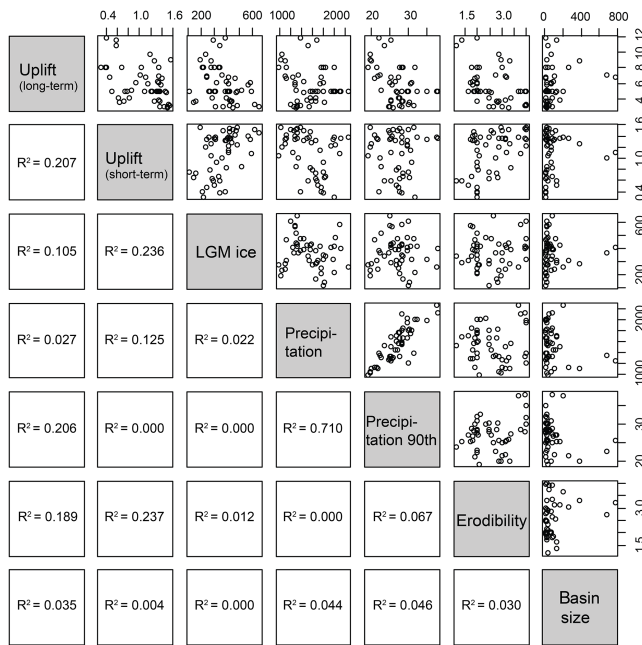


**Figure 7.** Correlation matrix of the possible controlling variables uplift (short- and long-term), precipitation (annual mean and 90th percentile), LGM ice thickness and erodibility. The strength of correlation for each pair is given by the square of the correlation coefficient,  $r^2$ .

amount of precipitation, topographic variables do not show any clear variation in between the three defined precipitation classes (Fig. 11). The only noticeable relation exists in wet basins ( $> 1836 \text{ mm year}^{-1}$ ), which are characterized by high elevations. For the intensity of precipitation, which we express here by the 90th percentile of daily precipitation, the results are also non-distinct (Fig. 12). However, the basins characterized by very high rainfall intensity show much steeper slopes than the basins with less intense precipitation.

Topographic variables show a relatively low scatter within the three erodibility groups, which is expressed by comparatively small boxes (Fig. 13). In particular, elevation, relief and slope values are significantly different between basins with high, medium and low erodibility. The relationships are less clear for hypsometric integral and river profile shapes.

#### 4.3 Linear discriminant analysis (LDA)

The LDA classification shows that the best results are generated when erodibility is considered as a classification basis (Table 3). In particular, 80 % of all basins are classified correctly on this basis, and the individual correct classification of the three groups ranges between c. 75 and 85 %. In the scatter plots, a clear clustering of the three classes is visible (Fig. 14). Basins with low and high erodibilities form distinct

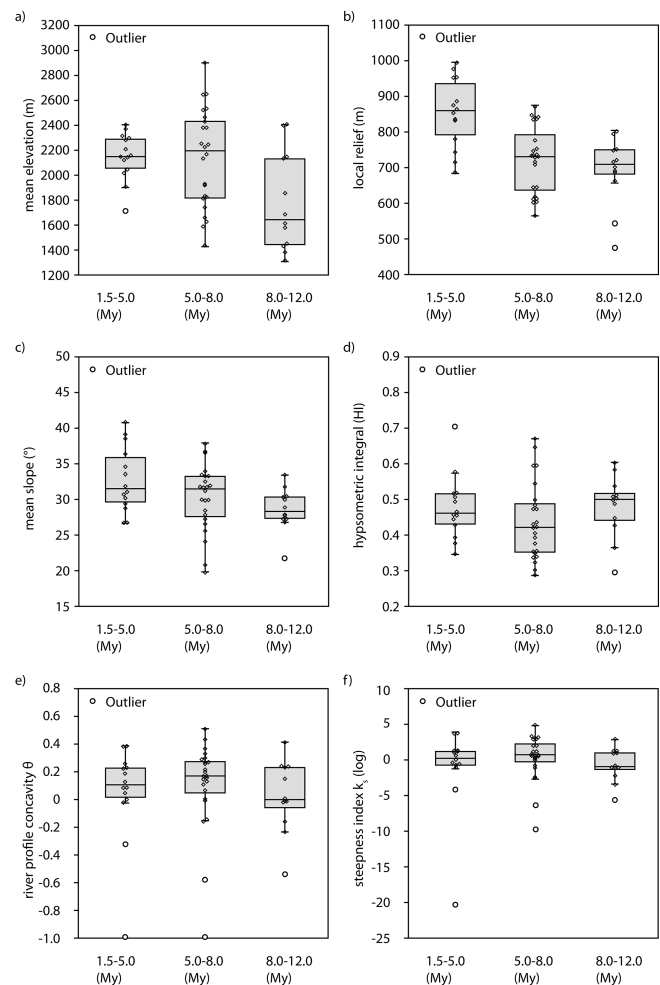


**Figure 8.** Boxplots of the topographic variables grouped according to the apatite fission-track ages (Vernon et al., 2008), which give long-term uplift information. The boxes represent the areas in which 50 % of the data plot (first and third quartile). The line in the middle is the median of the data. The whiskers mark the maximal and minimal value, and outliers are represented by white dots.

point clouds, while basins with a medium erodibility occur in between these clouds.

In the same sense, geodetic short-term uplift appears to be a good basis for clustering basins according to their landscape metrics, since a total of 76 % of basins are correctly classified. However, only 44 % of the basins in group 3 ( $1.4\text{--}1.6 \text{ mm year}^{-1}$ ) are classified correctly, which lowers the overall LDA performance. The clustering is clear in the scatter plots (Fig. 14). Note, however, that the cluster of basins of class 3 lies between the ones of classes 1 and 2.

Regarding the variables long-term uplift, LGM ice thickness and intensity of precipitation (90th percentile), the values of correct classifications range between 62 and 70 %. However, in all three cases, there is always one class that yields a very low percentage of correct classification. A clustering is hardly visible in the scatter plot for the variable



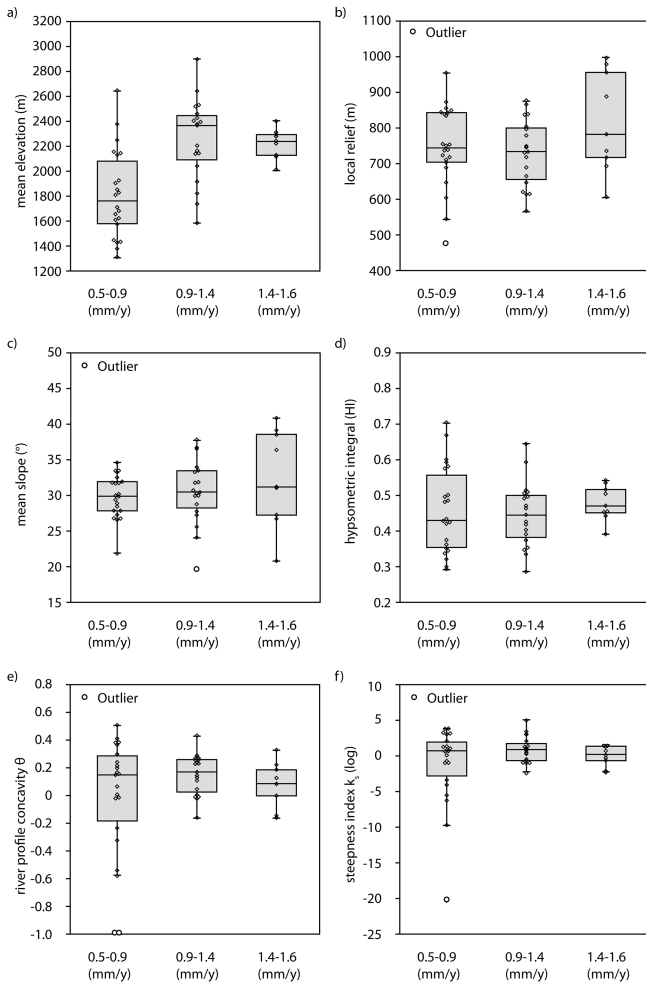


**Figure 9.** Boxplots of the topographic variables grouped according to the recent uplift rates (Schlatter et al., 2005), which give short-term uplift information.

long-term uplift and is mostly absent for the variables LGM ice thickness and intensity of precipitation. Finally, with respect to the amount of precipitation, all three classes of this variable yield percentages around 70 % if they are used as a categorization basis. However, in the scatter plots, clustering is rather poor as only class 3 forms a distinguishable point cloud, whereas the other two classes are indistinct from each other.

## 5 Discussion

Topographic metrics of tributary basins in the Rhône valley show relationships with all four controlling mechanisms (uplift, glacial inheritance, precipitation and erodibility). For example, river basins with a history of a relatively fast inferred exhumation rate (apatite FT cooling age < 5 My ago) have comparably higher elevation, relief and slope values, albeit with some poor correlations particularly regarding mean ele-

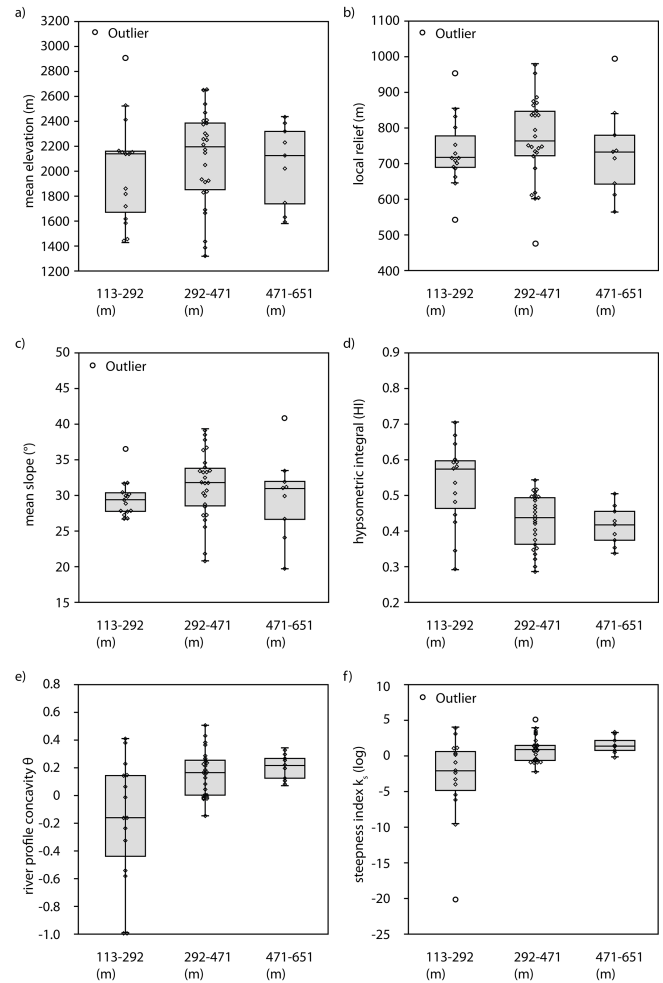


**Figure 10.** Boxplots of the topographic variables grouped according to the LGM ice thickness (Bini et al., 2009), which is indicative of glacial inheritance.

vation and local relief (Fig. 8). This trend is consistent with studies analysing the relationship between long-term surface uplift and the development of topography (e.g. Ahnert, 1984; Small and Anderson, 1998; Brocklehurst and Whipple, 2002). However, we could not find any significant relation between uplift (neither long-term nor short-term), hypsometry and river profile concavity. This suggests that the distribution of elevations within the basin and the shape of the river profile have not been influenced by uplift.

In contrast, we found a relation between hypsometry, river profile convexity and the LGM ice thickness, where basins with a thinner ice cover have higher hypsometric integrals and lower  $\theta$  values. Extensively glaciated basins characterized by thicker LGM ice can have lower equilibrium line altitudes (ELAs) than only moderately glaciated basins. This allows a stronger glacial modification especially in lower regions and thus a lowering of both the hypsometric curve and integral (Brocklehurst and Whipple, 2004). Ice thickness

**Table 3.** Results of the LDA classification based on the topographic variables for each of the controlling variables.

Uplift (long-term), in My ago					
Class	Classified as 1	Classified as 2	Classified as 3	Correctly classified	Total correct classification
1 (1.5–5.0)	9	5	0	64.29 %	66 %
2 (5.0–8.0)	3	19	2	79.17 %	
3 (8.0–12.0)	1	6	5	41.67 %	
Uplift (short-term), in mm year <sup>−1</sup>					
Class	Classified as 1	Classified as 2	Classified as 3	Correctly classified	Total correct classification
1 (0.5–0.9)	19	2	1	86.36 %	76 %
2 (0.9–1.4)	3	15	1	78.95 %	
3 (1.4–1.6)	1	4	4	44.44 %	
LGM ice thickness, in m					
Class	Classified as 1	Classified as 2	Classified as 3	Correctly classified	Total correct classification
1 (113–292)	8	7	0	53.33 %	62 %
2 (292–471)	3	23	0	88.46 %	
3 (471–651)	0	9	0	0 %	
Amount of precipitation (mean annual, in mm year <sup>−1</sup> )					
Class	Classified as 1	Classified as 2	Classified as 3	Correctly classified	Total correct classification
1 (975–1340)	14	6	9	70.00 %	70 %
2 (1340–1840)	6	15	0	71.43 %	
3 (1840–2278)	1	2	6	66.67 %	
Intensity of precipitation (90th percentile, in mm day <sup>−1</sup> )					
Class	Classified as 1	Classified as 2	Classified as 3	Correctly classified	Total correct classification
1 (19–25)	2	11	0	15.38 %	74 %
2 (25–31)	0	31	0	100 %	
3 (31–37)	0	2	4	66.67 %	
Erodibility					
Class	Classified as 1	Classified as 2	Classified as 3	Correctly classified	Total correct classification
1 (1–2, high)	17	4	0	80.95 %	80 %
2 (2–3, medium)	0	11	4	73.33 %	
3 (3–4, low)	1	1	12	85.71 %	

may influence the efficiency of glacial erosion in the valley through larger shear stresses driven by thick ice (Brocklehurst and Whipple, 2002; Dürst Stucki and Schlunegger, 2013). Thicker ice cover promotes the formation of flat and partially overdeepened lower reaches and steep head scarps, forming valleys with concave thalwegs. Large glacial erosion driven by thick ice may also promote fluvial incision during subsequent interglacial times through a positive feedback response (Norton et al., 2010b), where the landscape's disequilibrium, conditioned by glacial erosion, promotes fluvial erosion through headward retreat, thereby increasing the stream's concavity. This is expected along valley reaches where glacial processes resulted in the formation of topographic steps. In either case, glacial perturbations paired with

fluvial responses are expected to return thalwegs with larger concavities, which we invoke here to explain the positive correlations between these variables in the tributary basins of the Rhône River (Fig. 10e). Although variations in LGM ice cover seem to be a valid explanation for the shape of some of the observed river profiles and the elevation distributions within the basin (see also Schlunegger and Norton, 2013), we could not detect a relation between ice thickness and elevation, relief or slope. This suggests that in our study area the degree of glacial inheritance is not responsible for relief production or ridgeline lowering in the basins, nor can it be invoked to explain patterns of slope angles, as previously noted by Norton et al. (2010b).

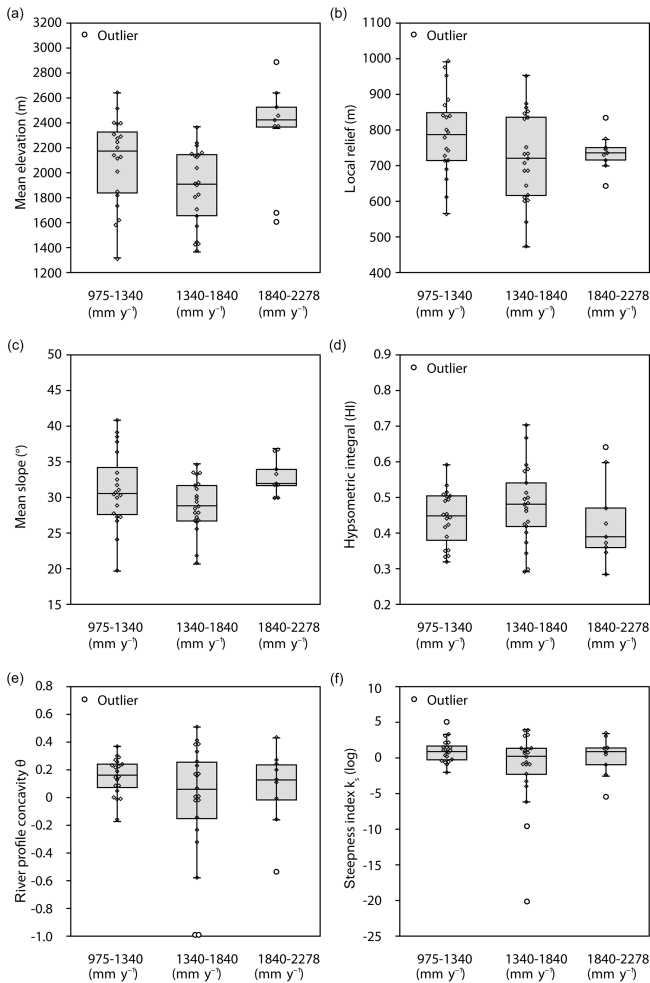


**Figure 11.** Boxplots of the topographic variables grouped according to the amount of precipitation, expressed by the annual mean precipitation.

Erodibility offers a possible explanation for reconciling some of the lack of correlations between landscape metrics, long-term uplift and LGM ice thickness outlined above. The main difference between the domains north and south of the Rhône River is their lithology and therefore their erodibility. Basins north of the Rhône are mainly underlain by lithologies of the Helvetic thrust nappes (erodibility classes 1–2) and the Aar massif (erodibility classes 3–4), while basins south of the Rhône are comprised of bedrock that is predominantly situated in Penninic thrust nappes (erodibility classes 2–3). Indeed, topographic variables show quite strong variation in between the three erodibility classes. Basins with low bedrock erodibility have higher elevation, relief and slope values than basins with a high erodibility. One factor influencing the erodibility of a rock is clearly the mechanical strength of the rocks, which has been inferred to be lower in carbonates than in granites or gneisses (Hoek and Brown, 1997; Kühni and Pfiffner, 2001). Rocks with a lower me-

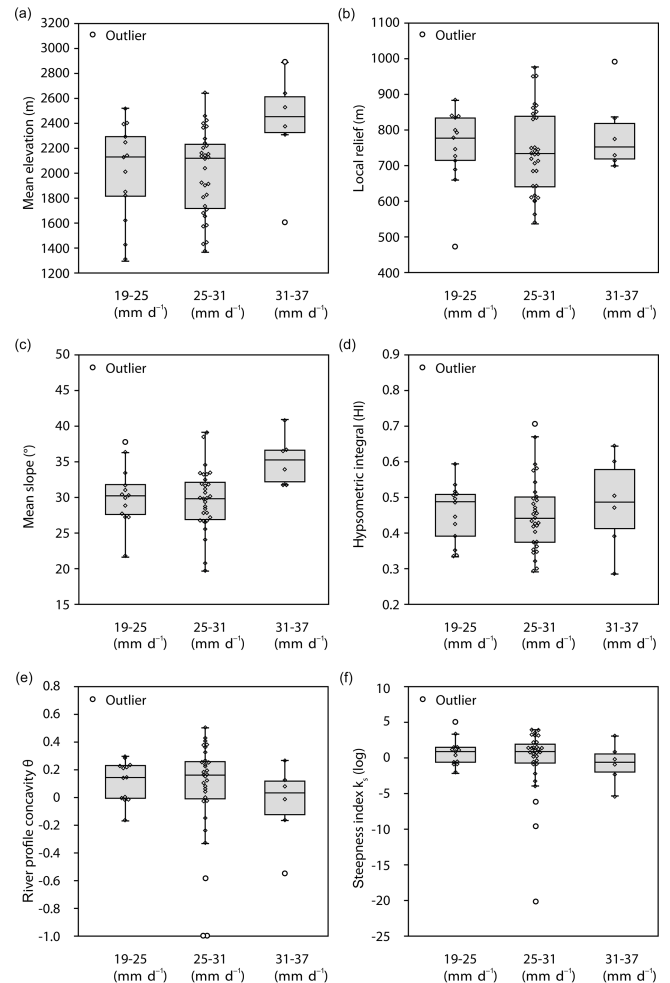


**Figure 12.** Boxplots of the topographic variables grouped according to the intensity of precipitation, expressed by the 90th percentile of total daily precipitation.

chanical strength are eroded more easily in response to rainfall, runoff and mass movements (Norton et al., 2011; Cruz Nunes et al., 2015), which over a long time span can result in a lowering of elevation. Furthermore, slopes underlain by a mechanically weak material are more prone to failure than lithologies with greater strengths, particularly in transient landscapes as is the case here. It is possible that mechanically weaker lithotypes are not able to sustain high hill-slope gradients over long periods of time (Kühni and Pfiffner, 2001).

Besides the mechanical rock strength itself, the susceptibility of the landscape towards erosion is also controlled by other factors including the structural fabric (faults, schistosity, bedding orientation) and seismicity (see, e.g., Persaud and Pfiffner, 2004; Molnar et al., 2007; Chittenden et al., 2014), as well as soil cover and potential for mass movements like landslides (Norton et al., 2010a; Korup and Schlunegger, 2009; Cruz Nunes et al., 2015). There is a spa-

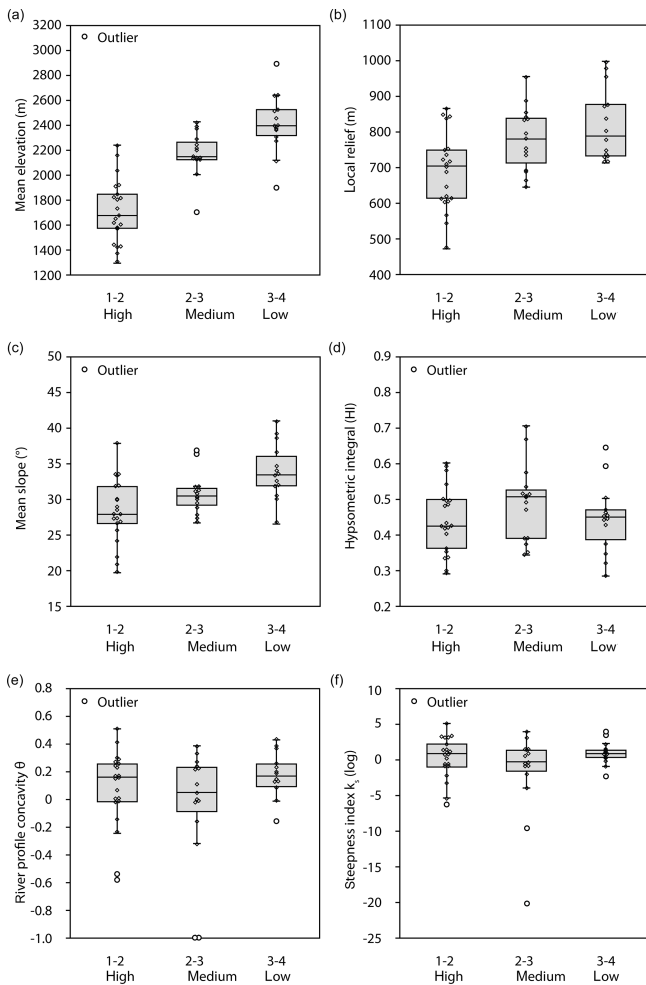


**Figure 13.** Boxplots of the topographic variables grouped according to erodibility.

tial clustering of earthquakes in the study area (Fig. 15), occurring most frequent northwest of the Rhône–Simplon lineament in the area of the Helvetic nappes. Most earthquakes show a strike-slip focal mechanism and occur along steep-dipping ENE–WSW to WNW–ESE trending faults (Maurer et al., 1997). In the Penninic nappes south of the Rhône–Simplon lineament, earthquakes show a wider spatial scatter and predominantly normal fault focal mechanisms. In contrast, earthquakes in the east of the study area occur more rarely, which coincides with the lack of large-scale tectonic faults (Fig. 15). Tonini et al. (2014) demonstrated that landslides are spatially clustered on the hillslopes bordering the Rhône valley and not in the tributary basins and that gravitational slope deformations are likely coupled to earthquakes. Furthermore, they observed that landslides occur predominantly in unconsolidated Quaternary material (mainly glacial till) and that former landslide material promotes new instabilities, thereby creating a positive feedback mechanism. Their map of landslides in the Rhône valley further shows a pattern

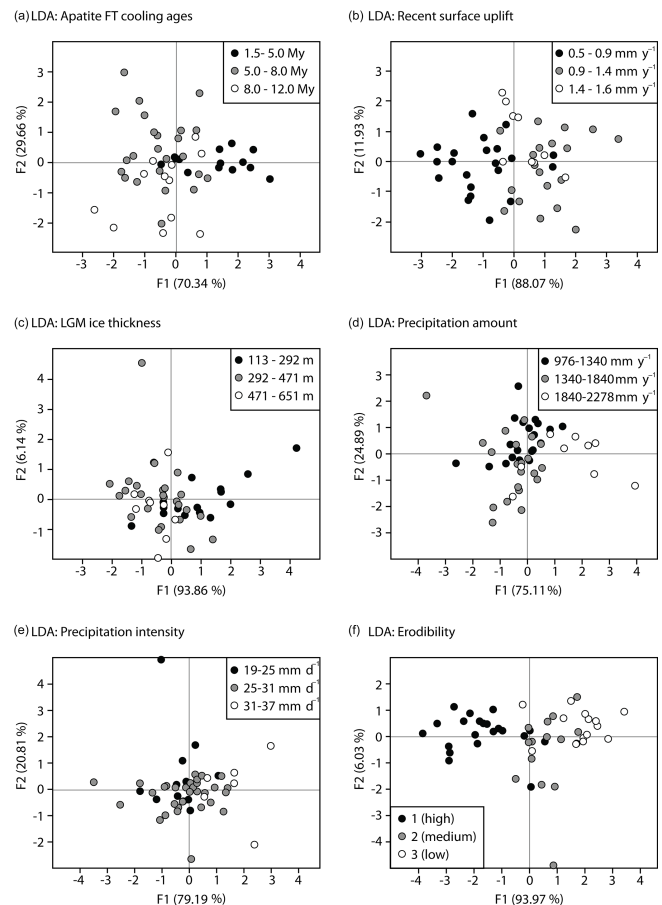


**Figure 14.** Scatter plots of the LDA results for long-term uplift (a), recent surface uplift (b), LGM ice thickness (c), amount (d) and intensity (e) of precipitation, and erodibility (f).

similar to the distribution of faults, earthquakes and quaternary deposits (Fig. 15), all of which are focused in the Helvetic nappes and near the lower elevations and valleys of the Penninic nappes.

Finally, the precipitation parameter is poorly correlated with any of the topographic characteristics. The only correlation with the precipitation and landscape metrics has been found for basins with very high precipitation rates, which appear to have generally high elevations, and also higher slope values. However, this is probably connected to the strong orographic effect in the Rhône Basin (Frei and Schär, 1998). Basins that are characterized by higher elevations experience on average more (and also more intense) rainfall than the basins located in lower and therefore more shielded locations. In this context, the precipitation is rather the effect of than the cause for the high elevations. Therefore, the topographic variables can be assumed to be largely independent of climatic conditions such as precipitation (Schlunegger and Norton, 2013).



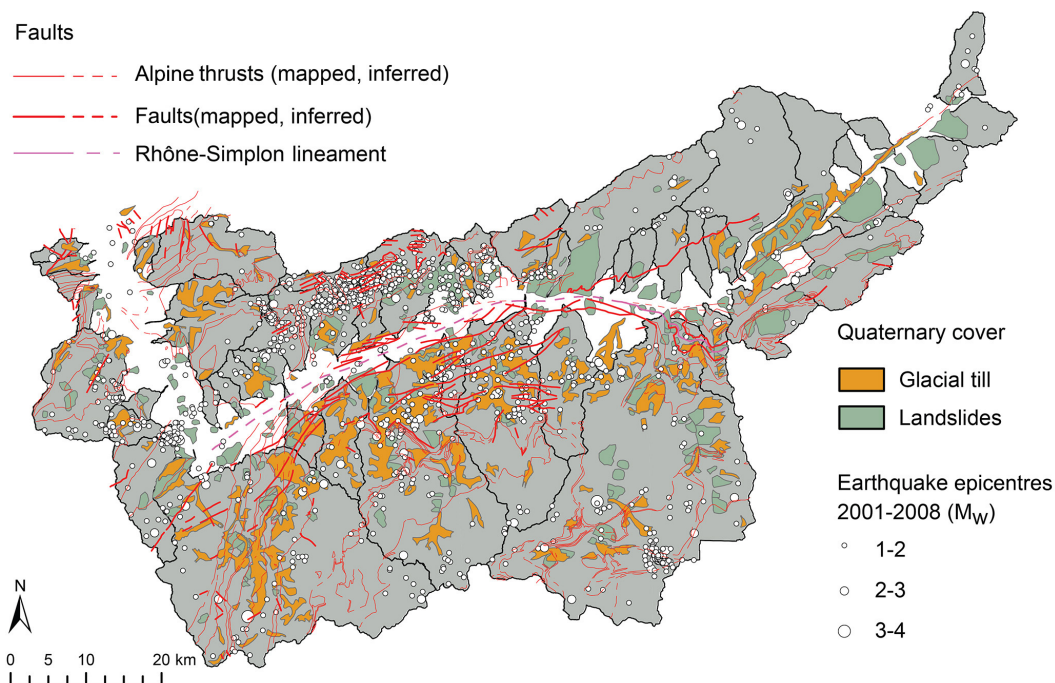


**Figure 15.** Compiled map of faults (geological map of Switzerland 1 : 25 000), earthquake epicentres (Swiss Earthquake Catalogue) and landslides (Tonini et al., 2014). For reasons of clarity, we display only the earthquake epicentres of a short time period. For the full data set and more detail about the data, see Fähr et al. (2011).

## 6 Conclusions

We used standard topographic variables including mean elevation, relief, slope, hypsometry and river profile concavity to characterize the topography of the Rhône Basin. A strong variation of these factors was observed between several sub-catchments. We therefore tested whether these differences can be explained by differences in uplift, glacial inheritance, precipitation conditions or erodibility. From boxplots and linear discriminant function analysis we found that the variation of variables can best be explained using the affiliation of the basins with the general erodibility of the underlying bedrock. However, we also found correlations of some topographic variables with glacial inheritance and uplift. In particular, we showed that uplift could be responsible for the development of elevation and relief in the study area, whereas the ice thickness during the LGM influenced the elevation distribution (hypsometry) of the basins, as well as the shape of some of the river profiles. We conclude, therefore, that although the landscape shows evidence of preconditioning effects related to uplift and glaciation, the high spatial variation of bedrock erodibility offers the best explanation for the observed patterns of landscape form in the Rhône Basin. In addition, the erodibility variable depends not only on the mechanical strength of the underlying bedrock but also on the fault and earthquake densities, as well as the potential for landslides.

**Acknowledgements.** We would like to thank Romain Delunel for help during field work and river profile analysis. We appreciated discussions with our project partners Maarten Bakker, Stéphanie Girardclos, Stuart Lane, Jean-Luc Loizeau, Peter Molnar and Tiago Adriaio Silva. We thank the editors, as well as J. D. Jansen and S. Brocklehurst, for their careful and comprehensive reviews, which greatly improved this manuscript.

This research was supported by the Swiss National Science Foundation (grant 147689).

Edited by: D. Lundbek Egholm

## References

- Adams, J.: Contemporary uplift and erosion of the Southern Alps, New Zealand, *Geol. Soc. Am. Bull.*, 91, 1–114, 1980.
- Ahnert, F.: Local relief and the height limits of mountain ranges, *Am. J. Sci.*, 284, 1035–1055, 1984.
- Baran, R., Friedrich, A. M., and Schlunegger, F.: The late Miocene to Holocene erosion pattern of the Alpine foreland basin reflects Eurasian slab unloading beneath the western Alps rather than global climate change, *Lithosphere*, 6, 124–131, 2014.
- Bennett, G., Molnar, P., Eisenbeiss, H., and McArdeell, B. W.: Erosional power in the Swiss Alps: characterization of slope failure in the Illgraben, *Earth Surf. Proc. Land.*, 37, 1627–1640, doi:10.1002/esp.3263, 2012.
- Bini, A., Buoncristiani, J.-F., Couterrand, S., Ellwanger, D., Felber, M., Florineth, D., Graf, H.R., Keller, O., Kelly, M., Schlüchter,

- C., and Schoeneich, P.: Switzerland during the last glacial maximum, *Swisstopo*, 1 : 50 000, Wabern, 2009.
- Brocklehurst, S. H. and Whipple, K. X.: Glacial erosion and relief production in the Eastern Sierra Nevada, California, *Geomorphology*, 42, 1–24, 2002.
- Brocklehurst, S. H. and Whipple, K. X.: Hypsometry of glaciated landscapes, *Earth Surf. Proc. Land.*, 29, 907–926, 2004.
- Brozović, N., Burbank, D. W., and Meigs, A. J.: Climatic Limits on Landscape Development in the Northwestern Himalaya, *Science*, 276, 571–574, 1997.
- Cederbom, C. E., van der Beek, P., Schlunegger, F., Sinclair, H. D., and Oncken, O.: Rapid extensive erosion of the North Alpine foreland basin at 5–4 Ma, *Basin Research*, 23, 528–550, 2011.
- Champagnac, J.-D., Molnar, P., Anderson, R. S., Sue, C., and Delacou, B.: Quaternary erosion-induced isostatic rebound in the western Alps, *Geology*, 35, 195–198, 2007.
- Champagnac, J.-D., Schlunegger, F., Norton, K. P., von Blanckenburg, F., Abbühl, L. M., and Schwab, M.: Erosion-driven uplift of the modern Central Alps, *Tectonophysics*, 474, 236–249, 2009.
- Champagnac, J.-D., Molnar, P., Sue, C., and Herman, F.: Tectonics, climate, and mountain topography, *J. Geophys. Res.*, 117, B02403, doi:10.1029/2011JB008348, 2012.
- Cheng, K.-Y., Hung, J.-H., Chang, H.-C., Tsai, H., and Sung, Q.-C.: Scale independence of basin hypsometry and steady state topography, *Geomorphology*, 171–172, 1–11, 2012.
- Chittenden, H., Delunel, R., Schlunegger, F., Akçar, N., and Kubik, P.: The influence of bedrock orientation on the landscape evolution, surface morphology and denudation ( $^{10}\text{Be}$ ) at the Niesen, Switzerland, *Earth Surf. Proc. Land.*, 39, 1153–1166, 2014.
- Cruz Nunes, F., Delunel, R., Schlunegger, F., Akçar, N., and Kubik, P.: Bedrock bedding, landsliding and erosional budgets in the Central European Alps, *Terra Nova*, 00, 1–10, 2015.
- Dürst Stucki, M. and Schlunegger, F.: Identification of erosional mechanisms during past glaciations based on a bedrock surface model of the central European Alps, *Earth Planet. Sc. Lett.*, 384, 57–70, 2013.
- Dürst Stucki, M., Schlunegger, F., Christener, F., Otto, J. C., and Götz, J.: Deepening of inner gorges through subglacial meltwater – An example from the UNESCO Entlebuch area, Switzerland, *Geomorphology*, 139, 506–517, 2012.
- Egli, D. and Mancktelow, N.: The structural history of the Mont Blanc massif with regard to models for its recent exhumation, *Swiss Journal for Geosciences*, 106, 469–489, 2013.
- England, P. and Molnar, P.: Surface uplift, uplift of rocks, and exhumation of rocks, *Geology*, 18, 1173–1177, 1990.
- Fäh, D., Giardini, D., Kästli, P., Deichmann, N., Gisler, M., Schwarz-Zanetti, G., Alvarez-Rubio, S., Sellami, S., Edwards, B., Allmann, B., Bethmann, F., Wössner, J., Gassner-Stamm, G., Fritsche, S., and Eberhard, D.: ECOS-09 Earthquake Catalogue of Switzerland Release 2011 Report and Database, Public catalogue, Swiss Seismological Service ETH Zürich, Report SED/RISK/R/001/20110417, 2011.
- Flint, J. J.: Stream Gradient as a Function of Order, Magnitude and Discharge, *Water Resour. Res.*, 10, 969–973, 1974.
- Florineth, D. and Schlüchter, C.: Reconstructing the Last Glacial Maximum (LGM) ice surface geometry and flowlines in the Central Swiss Alps, *Eclogae Geol. Helv.*, 91, 391–407, 1998.
- Fox, M., Herman, F., Kissling, E., and Willett, S. D.: Rapid exhumation in the Western Alps driven by slab detachment and glacial erosion, *Geology*, 43, 379–382, 2015.
- Frei, C. and Schär, C.: A precipitation climatology of the Alps from high-resolution rain-gauge observations, *Int. J. Climatol.*, 18, 873–900, 1998.
- Froitzheim, N., Schmid, S. M., and Frey, M.: Mesozoic paleogeography and the timing of eclogite-facies metamorphism in the Alps: A working hypothesis, *Eclogae Geol. Helv.*, 89, 81–110, 1996.
- Granger, D. E., Kirchner, J. W., and Finkel, R.: Spatially averaged long-term erosion rates measured from in situ-produced cosmogenic nuclides in alluvial sediment, *The Journal of Geology*, 104, 249–257, 1996.
- Gudmundsson, G.: An order-of-magnitude estimate of the current uplift-rates in Switzerland caused by the Wurm Alpine deglaciation, *Eclogae Geol. Helv.*, 87, 545–557, 1994.
- Hallett, B., Hunter, L., and Bogen, J.: Rates of erosion and sediment evacuation by glaciers: A review of field data and their implications, *Global and Planetary Change*, 12, 213–235, 1996.
- Hoek, E. and Brown, E. T.: Practical estimates of rock mass strength, *Int. J. Rock Mech. Min.*, 34, 1165–1186, 1997.
- Hurtrez, J.-E., Lucazeau, F., Lavé, J., and Avouac, J.-P.: Investigation of the relationships between basin morphology, tectonic uplift, and denudation from the study of an active fold belt in the Siwalik hills, central Nepal, *J. Geophys. Res.*, 104, 12779–12796, 1999.
- Ivy-Ochs, S., Kreschner, H., Reuther, A., Preusser, F., Heine, K., Maisch, M., Kubik, P. W., and Schlüchter, C.: Chronology of the last glacial cycle in the European Alps, *J. Quaternary Sci.*, 23, 559–573, 2008.
- Jäckli, H.: Gegenwartsgeologie des bündnerischen Rheingebietes, *Beitr. Geol. Schweiz*, 36, 136 pp., 1957.
- Jansen, J. D., Codilean, A. T., Stroeve, A. P., Fabel, D., Hättestrand, C., Kleman, J., Harbor, J. M., Heyman, J., Kubik, P. W., and Xu, S.: Inner gorges cut by subglacial meltwater during Fennoscandian ice sheet decay, *Nature communications*, 5, 3815, doi:10.1038/ncomms4815, 2014.
- Kahle, H. G., Geiger, A., Bürki, B., Gubler, E., Marti, U., Wirth, B., Rothacher, M., Gurtner, W., Beutler, G., Bauersima, I., and Pfiffner, O. A.: Recent crustal movements, geoid and density distribution: Contribution from integrated satellite and terrestrial measurements, in: Deep structure of the Swiss Alps: Results of NRP 20, edited by: Pfiffner, O. A., Lehner, P., Heitzmann, P., Müller, S., and Steck, A., Birkhäuser Verlag, Basel, 251–259, 1997.
- Kelly, M. A., Buoncristiani, J. F., and Schlüchter, C.: A reconstruction of the last glacial maximum (LGM) ice-surface geometry in the western Swiss Alps and contiguous Alpine regions in Italy and France, *Eclogae Geol. Helv.*, 97, 57–75, 2004.
- Korup, O.: Rock type leaves topographic signature in landslide-dominated mountain ranges, *Geophys. Res. Lett.*, 35, L11402, doi:10.1029/2008GL034157, 2008.
- Korup, O. and Montgomery, D. R.: Tibetan plateau river incision inhibited by glacial stabilization of the Tsangpo gorge, *Nature*, 455, 786–790, 2008.
- Korup, O. and Schlunegger, F.: Rock-type control on erosion-induced uplift, eastern Swiss Alps, *Earth Planet. Sc. Lett.*, 278, 278–285, 2009.

- Korup, O. and Weidinger, J. T.: Rock type, precipitation, and the steepness of Himalayan threshold hillslopes, *Geological Society, London, Special Publications*, 353, 235–249, 2011.
- Korup, O., Schmidt, J., and McSaveney, M. J.: Regional relief characteristics and denudation pattern of the western Southern Alps, *New Zealand, Geomorphology*, 71, 402–423, 2005.
- Kuhlemann, J., Frisch, W., Székely, B., Dunkl, I., and Kázmér, M.: Post-collisional sediment budget history of the Alps: tectonic versus climatic control, *Int. J. Earth Sci.*, 91, 818–837, 2002.
- Kühni, A. and Pfiffner, O. A.: The relief of the Swiss Alps and adjacent areas and its relation to lithology and structure: topographic analysis from a 250-m DEM, *Geomorphology*, 41, 285–307, 2001.
- Maurer, H. R., Burkhard, M., Deichmann, N., and Green, A. G.: Active tectonism in the central Alps: contrasting stress regimes north and south of the Rhone Valley, *Terra Nova*, 9, 91–94, 1997.
- McLachlan, G. J.: Discriminant analysis and statistical pattern recognition, Wiley Interscience, New York, 552 pp., 2004.
- Michalski, I. and Soom, M.: The Alpine thermo-tectonic evolution of the Aar and Gotthard massifs, Central Switzerland: Fission Track ages on zircon and apatite and K-Ar mica ages, *Schweizerische mineralogische und petrographische Mitteilungen*, 70, 373–388, 1990.
- Molnar, P., Anderson, R. S., and Anderson, S. P.: Tectonics, fracturing of rock, and erosion, *J. Geophys. Res.*, 112, F03014, doi:10.1029/2005JF000433, 2007.
- Montgomery, D. R.: Valley formation by fluvial and glacial erosion, *Geology*, 30, 1047–1050, 2002.
- Montgomery, D. R. and Brandon, M. T.: Topographic controls on erosion rates in tectonically active mountain ranges, *Earth Planet. Sc. Lett.*, 201, 481–489, 2002.
- Montgomery, D. R., Balco, G., and Willett, S. D.: Climate, tectonics, and the morphology of the Andes, *Geology*, 29, 579–582, 2001.
- Morel, P., von Blanckenburg, F., Schaller, M., Kubik, P. W., and Hinderer, M.: Lithology, landscape dissection and glaciation controls on catchment erosion as determined by cosmogenic nuclides in river sediment (the Wutach Gorge, Black Forest), *Terra Nova*, 15, 398–404, 2003.
- Niggli, P. and de Quervain, F. D.: *Geotechnische Karte der Schweiz*. Schweizerische Geotechnische Kommission, Kümmerly and Frey, Geotechnischer Verlag, Bern, 1936.
- Norton, K. P., von Blanckenburg, F., and Kubik, P. W.: Cosmogenic nuclide-derived rates of diffusive and episodic erosion in the glacially sculpted upper Rhone Valley, Swiss Alps, *Earth Surf. Proc. Land.*, 35, 651–662, 2010a.
- Norton, K. P., Abbühl, L. M., and Schlunegger, F.: Glacial conditioning as an erosional driving force in the Central Alps, *Geology*, 38, 655–658, 2010b.
- Norton, K. P., von Blanckenburg, F., DiBiase, R., Schlunegger, F., and Kubik, P. W.: Cosmogenic  $^{10}\text{Be}$ -derived denudation rates of the Eastern and Southern European Alps, *Int. J. Earth Sci.*, 100, 1163–1179, 2011.
- Persaud, M. and Pfiffner, O. A.: Active deformation in the eastern Swiss Alps: post-glacial faults, seismicity and surface uplift, *Tectonophysics*, 385, 59–84, 2004.
- Pfiffner, O. A., Sahli, S., and Stäubli, M.: Compression and uplift of the external massifs in the Helvetic zone, in: *Deep Structure of the Swiss Alps: Results of NRP 20*, Pfiffner, O. A., Lehner, P., Heitzmann, P., Müller, S., and Steck, A., Birkhäuser, Switzerland, 139–153, 1997.
- Robl, J., Prasicek, G., Hergarten, S., and Stüwe, K.: Alpine topography in the light of tectonic uplift and glaciation, *Global and Planetary Change*, 127, 34–49, 2015.
- Schaller, M., von Blanckenburg, F., Hovius, N., and Kubik, P. W.: Large-scale erosion rates from in situ-produced cosmogenic nuclides in European river sediments, *Earth Planet. Sc. Lett.*, 188, 441–458, 2001.
- Scharf, T. E., Codilean, A. T., De Wit, M., Jansen, J. D., and Kubik, P. W.: Strong rocks sustain ancient postorogenic topography in southern Africa, *Geology*, 41, 331–334, 2013.
- Schlatter, A., Schneider, D., Geiger, A., and Kahle, H. G.: Recent vertical movements from precise levelling in the vicinity of the city of Basel, Switzerland, *Int. J. Earth Sci.*, 94, 507–514, 2005.
- Schlunegger, F. and Hinderer, M.: Crustal uplift in the Alps: why the drainage pattern matters, *Terra Nova*, 13, 425–432, 2001.
- Schlunegger, F. and Norton, K. P.: Water versus ice: The competing roles of modern climate and Pleistocene glacial erosion in the Central Alps of Switzerland, *Tectonophysics*, 602, 370–381, 2013.
- Schlunegger, F. and Willett, S. D.: Spatial and temporal variations in exhumation of the Central Swiss Alps and implications for exhumation mechanisms, in: *Exhumation processes: normal faulting, ductile flow, and erosion*, edited by: Ring, U., Brandon, M. T., Lister, G. S., and Willett, S. D., Geological Society of London Special Publication, 154, 157–180, 1999.
- Schmid, S. M., Pfiffner, O. A., Froitzheim, N., Schönborn, G., and Kissling, E.: Geophysical-geological transect and tectonic evolution of the Swiss-Italian Alps, *Tectonics*, 15, 1036–1064, 1996.
- Schmid, S. M., Fügenschuh, B., Kissling, E., and Schuster, R.: Tectonic map and overall architecture of the Alpine orogen, *Eclogae Geol. Helv.*, 97, 93–117, 2004.
- Schwanghart, W. and Kuhn, N. J.: TopoToolbox: a set of Matlab functions for topographic analysis, *Environ. Modell. Softw.*, 25, 770–781, 2010.
- Schwarb, M.: *The Alpine Precipitation Climate Evaluation of a High-Resolution Analysis Scheme using Comprehensive Rain-Gauge Data*, PhD thesis, ETH Zurich, Switzerland, 131 pp., 2000.
- Seward, D. and Mancktelow, N. S.: Neogene kinematics of the central and western Alps: Evidence from fission-track dating, *Geology*, 22, 803–806, 1994.
- Shuster, D. L., Ehlers, T. A., Rusmore, M. E., and Farley, K. A.: Rapid glacial erosion at 1.8 Ma revealed by  $^4\text{He}/^3\text{He}$  thermochronology, *Science*, 310, 1668–1670, 2005.
- Small, E. E. and Anderson, R. S.: Pleistocene relief production in Laramide mountain ranges, western United States, *Geology*, 26, 123–126, 1998.
- Snyder, N. P., Whipple, K. X., Tucker, G. E., and Merritts, D. J.: Landscape response to tectonic forcing: DEM analysis of stream profiles in the Mendocino triple junction region, northern California, *Geol. Soc. Am. Bull.*, 112, 1250–1263, 2000.
- Spotila, J. A., Buscher, J. T., Meigs, A. J., and Reiners, P. W.: Long-term glacial erosion of active mountain belts: Example of the Chugach-St. Elias Range, Alaska, *Geology*, 32, 501–504, 2004.
- Strahler, A. N.: Hypsometric (area-altitude) analysis of erosional topography, *Bull. Geol. Soc. Am.*, 63, 1117–1142, 1952.

- Stüwe, K., White, L., and Brown, R.: The influence of eroding topography on steady-state isotherms. Application to fission track analysis, *Earth Planet. Sc. Lett.*, 124, 63–74, 1994.
- Sue, C., Delacou, B., Champagnac, J.-D., Allan, C., Tricart, P., and Burkhard, M.: Extensional neotectonics around the bend of the western/central Alps: An overview, *Int. J. Earth Sci.*, 96, 1101–1129, 2007.
- Tonini, M., Pedrazzini, A., Penna, I., and Jaboyedoff, M.: Spatial pattern of landslides in Swiss Rhone Valley, *Natural Hazards*, 73, 97–110, 2014.
- Valla, P. G., Shuster, D. L., and van der Beek, P.: Significant increase in relief of the European Alps during mid-Pleistocene glaciations, *Nature Geosciences*, 4, 688–692, 2011.
- Vernon, A. J., van der Beek, P. A., Sinclair, H. D., and Rahn, M. K.: Increase in late Neogene denudation of the European Alps confirmed by analysis of a fission-track thermochronology database, *Earth Planet. Sc. Lett.*, 270, 316–329, 2008.
- Whipple, K. X.: Bedrock rivers and the geomorphology of active orogens, *Annu. Rev. Earth Pl. Sc.*, 32, 151–185, 2004.
- Whipple, K. X. and Tucker, G. E.: Dynamics of the stream-power river incision model: Implications for the height limits of mountain ranges, landscape response time scales, and research needs, *J. Geophys. Res.*, 104, 17661–17674, 1999.
- Willett, S. D.: Orogeny and orography: The effects of erosion on the structure of mountain belts, *J. Geophys. Res.*, 104, 28957–28981, 1999.
- Willett, S. D. and Brandon, M. T.: On steady states in mountain belts, *Geology*, 30, 175–178, 2002.
- Willett, S. D., Schlunegger, F., and Picotti, V.: Messinian climate change and erosional destruction of the central European Alps, *Geology*, 34, 613–616, 2006.
- Willgoose, G. and Hancock, G.: Revisiting the hypsometric curve as an indicator of form and process in transport-limited catchment, *Earth Surf. Proc. Land.*, 23, 611–623, 1998.
- Wischmeier, W. H.: A Rainfall Erosion Index for a Universal Soil-Loss Equation, *Soil Sci. Soc. Am. J.*, 23, 246–249, doi:10.2136/sssaj1959.036159950023000300027x, 1959.
- Wittmann, H., von Blanckenburg, F., Kruesmann, T., Norton, K. P., and Kubik, P. W.: Relation between rock uplift and denudation from cosmogenic nuclides in river sediment in the Central Alps of Switzerland, *J. Geophys. Res.*, 112, F04010, doi:10.1029/2006JF000729, 2007.
- Wobus, C., Whipple, K. X., Kirby, E., Snyder, E., Johnson, J., Spyropoulou, K., Crosby, B., and Sheehan, D.: Tectonics from topography: Procedures, promise, and pitfalls, in: *Tectonics, climate, and landscape evolution*, edited by: Willett, S. D., Hovius, N., Brandon, M. T., and Fisher, D. M., Geological Society of America Special Paper, Boulder, Colorado, USA, 398, 55–74, 2006.